*Article*

# Mechanical Behavior of Crimping Composite Post Insulator : Experimental and Simulation Study

**Jin Xiao [1, 2], Yanhong Zhang [1,*], Yichuan Xing [1], Yangyang Jiao [2] and Lihong Zhang [1]**

[1] State Key Laboratory of Simulation and Regulation of Water Cycle in River Basin, China Institute of Water Resources and Hydropower Research, Beijing, 100044,China.; xiaojinxjgc@163.com
[2] Xuji Electric Co., Ltd, Xuchang, 461000, China
* Correspondence: zhangyh@iwhr.com

**Abstract:** The composite post insulator composed of a large diameter mandrel and flange pressed by one-time integral pultrusion has high strength and good toughness, widely used in the existing flexible converter valve. For constructing the finite element model of the crimped post insulator, most of the flange surface and the mandrel surface are directly connected, making the simulation model's stiffness deviate from the actual model and the model distortion. Based on this, this study proposes a new finite element simplified model of crimped composite post insulator based on Multi-Point Constraints (MPC), which accurately simulates the crimping area of mandrel and flange in engineering practice. It verifies the model's reliability through static tests and characteristic vibration tests. The results show that the difference between the finite element simulation and test results is within 5 %. The finite element modeling method based on MPC local constraints is very reliable in applying crimped composite post insulators.

Based on the proposed model, the influence of flange height and thickness on the mechanical properties of composite post-insulators is further explored. The results show that the influence of flange height on mechanical properties can be ignored when the height of the insulator stiffener ( non-press common area ) is constant. Within the allowable thickness range of the flange crimping process, the increase in flange thickness will significantly reduce the maximum bending stress of the insulator and increase its safety margin. It provides a good design idea for the design of crimping composite insulators.

**Keywords:** composite post insulator; dynamic performance test; flexible high voltage direct current (HVDC) converter valve; finite element analysis, mechanical property

## 1. Introduction

Seismic damage data of power systems worldwide shows that earthquakes easily damage all high-voltage electrical equipment in substations[1-4]. Due to the obvious comprehensive advantages of comp006Fsite materials, such as strong impact resistance, good fracture toughness and anti-burst performance, large self-damping and earthquake resistance, composite pillar insulators have been used in the substation and converter stations since 2000 [5-7]. However, the research on the mechanical mechanics, dynamic characteristics, and seismic capacity evaluation of composite electrical equipment worldwide still needs to be stronger. With the rapid development of the ultra-high voltage (UHV) direct current (DC) transmission grid in recent years, most of the equipment in the converter station is supported by pillar insulators, which not only provide electrical insulation for electrical equipment but also serve as structural support. In addition to the mechanical stress, it also bears complex electrical stress, so the reliability of the pillar insulator plays a crucial role in the stable operation of the substation's electrical equipment[8, 9]. At present, pillar insulators are widely used in substations, converter stations, or power distribution devices as the fixing and insulating support components of high-voltage busbars, such as flexible DC converter valves, busbar pillars, isolation switches, smoothing reactors, and other occasions[10, 11].

At the beginning of the 21st century, large-diameter composite post insulator mainly adopts hollow composite material[10, 12, 13]. A.M.Reinhorn conducted mechanical performance tests on hollow composite post insulators and pointed out the main structural failure modes of post

Preprints (www.preprints.org) | NOT PEER-REVIEWED | Posted: 21 April 2023 doi:10.20944/preprints202304.0693.v1

composite insulators in 2009[14, 15]. Rao Hong studied the ±800kV DC post composite insulators with a small diameter mandrel as the base shaft, which was wound and cured into a large-diameter mandrel, and a high-temperature vulcanized silicone rubber adhered to the periphery of the mandrel[16]. End flanges bonded with adhesive and mandrel with sealing measures. Composite post insulators are mainly subjected to bending, torsion, and mechanical compression loads[17]. Based on this, He Faliang studied the assembly and connection of end flange fittings and large-diameter cores by crimping process, which solved the problem of excessive offset value caused by existing glued post composite insulators under bending load[18]. The crimping process's characteristics are that the mandrel's outer diameter and the flange's inner diameter adopt a sliding fit size. In the production process of insulators, use six claw or eight-claw automatic hydraulic crimping machine on the outer diameter of the flange with uniform pressure so that the flange is firmly crimped on the mandrel to complete crimping. In recent years, the mandrel process of single-piece pultrusion with large diameters below 220mm has become increasingly mature and replaced hollow composite post insulators in batches. It is widely used in flexible DC projects. Compared with hollow composite post insulators, one-time pultrusion the diameter mandrel insulator has simpler processing technology, and the process reliability of the product is greatly improved. Therefore, the large diameter mandrel and flange integral crimping by one-time integral pultrusion will be the main development of composite post insulators in trend[19, 20].

The flexible DC converter valve comprises hundreds of insulators to form a structural frame, and the valve components equipped with power components are stacked in horizontal and vertical directions[2]. The converter valve is the core of electric equipment, and its structure size and weight are large. Especially the flexible converter valve, which weighs nearly one hundred tons, the reliability analysis of the converter valve support structure is of great significance. At present, the seismic analysis of the converter valve is mainly carried out utilizing finite element simulation analysis. As the most important structural support component of the flexible DC converter valve, the accuracy of the finite element model of the composite post-insulator will have a crucial impact on the overall structural characteristics of the flexible DC converter valve[21]. The composite post insulator is the most important structural support component of the flexible DC converter valve, and the accuracy of its finite element model will have a crucial impact on the overall structural characteristics of the flexible DC converter valve. Currently, most simulation studies on post insulators as supporting components focus on glue-mounted post insulators[22, 23], while the simulation analysis of crimped composite post insulators still needs to be improved.

Furthermore, the researchers usually directly connect the flange surface with the mandrel surface by the rigid constraint in the seismic simulation analysis of engineering structures[24, 25]. They usually ignore the lateral stiffness of the insulator connection section, which leads to a deviation between the simulation model and the actual situation.

To solve the distortion problem of the crimped composite post-insulator model, this paper proposes a new simulation model method for constructing crimped composite insulators. This paper uses the MPC local constraint method to simulate the crimping area of the insulator rod and flange. The accuracy and reliability of the modeling method are demonstrated by comparing the mechanical performance experiment with the simulation analysis results, which provides a solution for the accurate modeling of the structure in the flexible DC converter valve. Furthermore, according to this modeling method, the height and thickness parameters of the flange are designed and optimized. Specifically, the influence of flange height and thickness parameters on the mechanical properties is explored, providing essential data for the processing and production of crimped composite insulators.

**Table 1.** Main Material Parameter.

| Material | Elastic modulus /GPa | Density /(kg·m$^{-3}$) | Poisson ratio |
|---|---|---|---|
| Mandrel | 45.5 | 2150 | 0.21 |
| Flange | 140 | 7850 | 0.30 |

Preprints (www.preprints.org) | NOT PEER-REVIEWED | Posted: 21 April 2023 doi:10.20944/preprints202304.0693.v1

## 2. Modeling

### *2.1. Simplified mechanical model*

Currently, the flexible DC converter valve is mainly supported on the valve hall ground by composite post insulators[26]. Each layer of the converter valve is vertically supported by a composite post insulator to form the main structural support frame, thereby realizing the flexible converter valve's structural support and electrical insulation. Fig. 1 shows a project flexible DC converter valve. The composite post insulator mainly comprises a flange, core rod, and silicone rubber shed. In this paper, composite post insulators supported at the bottom of a flexible converter valve are selected as the research object, and their dimensions are shown in Fig. 2.

The insulator length is 2750 mm, and the rod diameter is 183mm. The mandrel is made of reinforced glass fiber epoxy resin by integral pultrusion. The flange is made of cast steel. The crimping process fixes the flange and mandrel. Table 1 shows the main material parameters of composite post-insulators.

The insulator length is 2750 mm, and the rod diameter is 183mm. The mandrel is made of reinforced glass fiber epoxy resin by integral pultrusion. The flange is made of cast steel. The crimping process fixes the flange and mandrel. Table 1 shows the main material parameters of composite post-insulators.

**Figure 1.** Flexible direct current converter valve of some project.

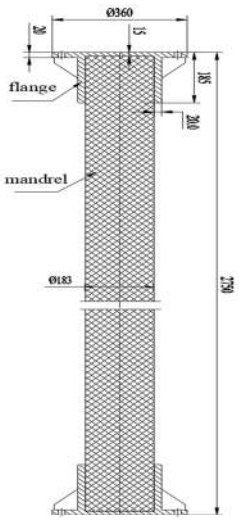


**Figure 2.** Flexible Outline drawing of the insulator.

Preprints (www.preprints.org) | NOT PEER-REVIEWED | Posted: 21 April 2023 doi:10.20944/preprints202304.0693.v1

Because the silicone rubber sheds coated on the outer side of the composite post insulator play an electrical insulation role[12], the influence on the structural strength can be ignored entirely. Therefore, the mechanical performance analysis of this paper does not consider the silicone rubber umbrella skirt.

According to the stress analysis and structural characteristics of composite post insulator, the deflection of the insulator is far less than its length. In other words, when the bending radius is much larger than the height of the insulator, the bending deformation is dominant, so the mechanical model of the insulator can be equivalent to the Euler-Bernoulli beam theory[13]. The free vibration equation of an insulator is:

$$M\frac{\partial^2 u}{\partial t^2}+\frac{\partial^2}{\partial x^2}\left[EI\frac{\partial^2 u}{\partial x^2}\right]=0 \tag{1}$$

Solve equation (1) by the method of separating variables, assuming that the form of the solution is:

$$u(x,t)=\phi(x)q(t) \tag{2}$$

In (2), $\phi(x)$ represents the shape of the vibration, which does not change with time. $q(t)$ represents the amplitude changing with time. Substitute (2) into (1), and we can get

$$\phi''''(x)-\frac{\omega^2 M}{EI}\phi(x)=0 \tag{3}$$

One end of the insulator is fixed, and the other is free. It can be equivalent to a cantilever beam, as shown in Fig. 3.

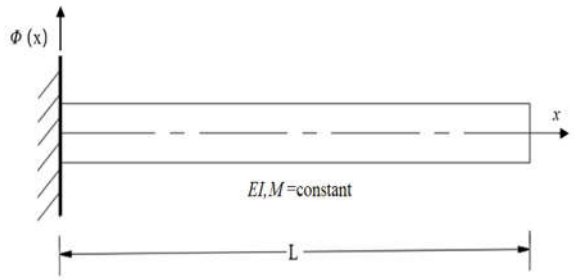


**Figure 3.** Cantilever.

The boundary conditions are: At $x$=0, its displacement and rotation angle are zero, that is $\phi(0)$=0, $\phi'(0)$=0. At x=L, its bending moment and shear force are zero, that is $\phi''(L)$=0, $\phi'''(L)$=0. The above can be solved.

$$\omega_1=3.516\sqrt{\frac{EI}{ML^4}} \tag{4}$$

$$\omega_2=22.03\sqrt{\frac{EI}{ML^4}} \tag{5}$$

For single composite post insulator, $L$=2.75m, $E$=4.55·10$^{10}$Pa, $M$=87.45kg/m, $I$=5.505·10$^{-5}$m$^4$. Bringing it into (4) and (5), we can get $\omega_1$=78.68rad/s, $\omega_2$=493.1rad/s. The corresponding first two natural frequencies are $f_1$=12.5Hz, and $f_2$=78.5Hz. Two insulators are connected in series along the vertical direction. From (4) and (5), the first two natural frequencies are 3.2Hz and 20Hz.

Preprints (www.preprints.org) | NOT PEER-REVIEWED | Posted: 21 April 2023 doi:10.20944/preprints202304.0693.v1

*2.2. Finite element model*

In this chapter, the finite element analysis software ANSYS is used for the numerical analysis of single and two composite post insulators. Specifically, extracting the center surface of the flange, the surface unit is used to replace the body unit in the solid flange model. Extracting the center line of the rod, the line unit replaces the body unit in the solid rod model. The simplified insulator model is shown in Fig. 4.

(a) (b)

**Figure 4.** Simplified finite element model (a) single insulator (b) two insulator strings.

According to the flange crimping process, the position of the flange stiffener is the non-pressing part. The upper part of the flange stiffener is the critical part, as shown in Fig. 5. To simulate the contact between the mandrel and the flange crimping part more accurately, the contact pair between the mandrel and the flange inner wall is defined. The inner wall of the flange is used as the target surface, and the surface of the mandrel is used as the contact surface. The MPC local constraint method is used to constrain the multi-point of the crimping section, while the non-pressed parts take free contact, as shown in Fig.6.

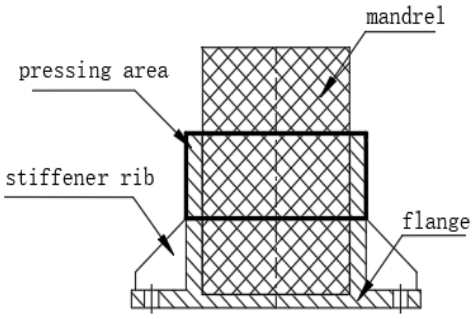


**Figure 5.** Schematic drawing of flange.

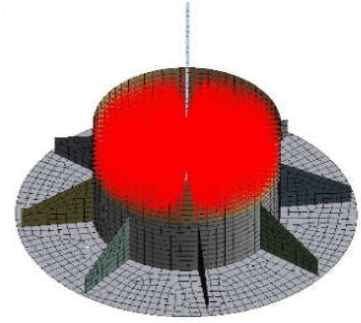

**Figure 6.** Local MPC constraint between flange and pressed position core rod.

**Table 2.** Results Comparison in Different Modeling Methods

| Model | The first order natural frequency/Hz | 2nd order natural frequency/Hz |
|---|---|---|
| Theoretical calculation of single insulator | 12.50 | 78.50 |
| Model of single insulator | 12.50 | 87.90 |
| Theoretical calculation of two insulators | 3.20 | 20.00 |
| Model of two insulators | 3.26 | 19.69 |

Preprints (www.preprints.org) | NOT PEER-REVIEWED | Posted: 21 April 2023 doi:10.20944/preprints202304.0693.v1

As shown in Table 2, comparing the simulation model with the theoretical calculation results, it is found that the calculation results of the simulation model are similar to the theoretical calculation. That is, the fitting degree is high. There is a deviation between the simulation analysis and the theoretical calculation of the second-order natural frequency. The main reason is that the theoretical calculation does not consider the influence of the flange, so the second-order natural frequency is minor.

### *2.3. Experimental verification of statics*

To verify the accuracy of the finite element model, this paper carried out a single insulator static tensile test. The 1# and 2# single insulators are installed on the 25 mm thick steel plate and fixed on the shaking table. The horizontal tension is applied to the top flange of the two insulators, increasing from 0.5kN to 4.5kN in turn. Tensile force sensors are used to control the pull force. There are five channels in the test, as shown in Table 3. The experiment was repeated four times. Strain measuring points are arranged on two sides of the core rod. The strain measuring points are about 40 mm from the top of the flange. The microstrain of the insulator core under different tension is measured. The elastic modulus of the insulator core and the stress at the corresponding measuring position can be obtained by data processing.

Table 4 shows the measured elastic modulus and Poisson's 1# and 2# insulator cores ratio. The average elastic modulus of 1# insulator rod is 47.278GPa, and Poisson's ratio is 0.210. The average elastic modulus of 2# insulator rod is 45.462GPa, and Poisson's ratio is 0.212. The difference in elastic modulus and Poisson's ratio between the two insulator rods is less than 4 %, so the consistency is good.

**Table 3.** Strain Test Point and Force Test Point

| Measure point | Position | Direction | Channel |
|---|---|---|---|
| S2X-W | 1# insulator bottom west side X direction | 90° | 1 |
| S2X-E | 1# insulator bottom east side X direction | 90° | 2 |
| S3X-W | 2# insulator bottom west side X direction | 90° | 3 |
| S3X-E | 2# insulator bottom east side X direction | 90° | 4 |
| Force | guy rope | horizon | 5 |

**Table 4.** Elastic Modulus and Poisson's Ratio of 1# and 2# Insulator Rod

| Loading times | 1# insulator | | 2# insulator | |
|---|---|---|---|---|
| | Elastic modulus/GPa | Poisson's ratio | Elastic modulus/GPa | Poisson's ratio |
| 1 | 47.234 | 0.208 | 45.584 | 0.210 |
| 2 | 47.335 | 0.208 | 45.458 | 0.210 |
| 3 | 47.268 | 0.212 | 45.406 | 0.208 |
| 4 | 47.274 | 0.211 | 45.399 | 0.211 |
| average | 47.278 | 0.210 | 45.462 | 0.212 |

In order to further explore the mechanical gap between two insulator rods, Fig.7 shows the stress-strain curves of two insulators under horizontal tension from 0.5kN to 4.5kN. The stress-strain curves of the two insulator cores are in good agreement, so their static properties are similar.

Preprints (www.preprints.org) | NOT PEER-REVIEWED | Posted: 21 April 2023 doi:10.20944/preprints202304.0693.v1

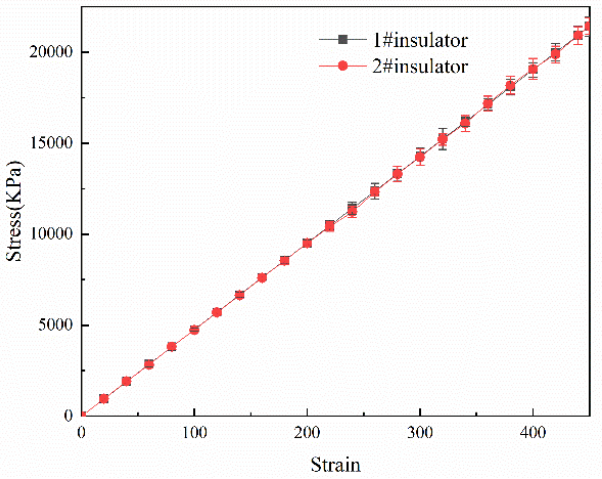


**Figure 7.** Stress-strain curves of 1# and 2# insulator rod.

Based on the above experimental conclusions, the finite element model constructed in section 2.2 is further fitted. Fig. 8 shows the stress distribution diagram of the insulator under the horizontal tension of 4.5 kN. Fig. 9 is the stress-strain curve comparison diagram of the insulator core rod root under horizontal tension from 0.5 kN to 4.5 kN. The experimental and simulation results are very close, and the error range is within 5%.

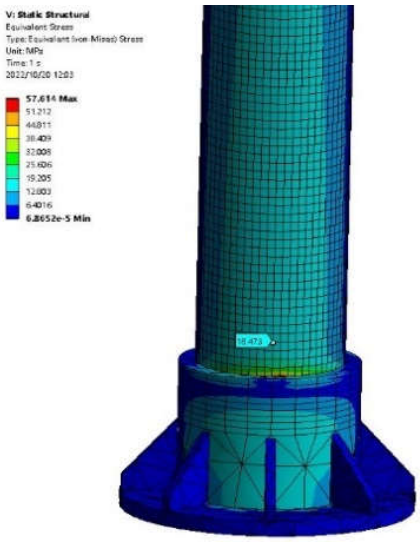


**Figure 8.** The mandrel under a horizontal tension of 4.5 KN.

Preprints (www.preprints.org) | NOT PEER-REVIEWED | Posted: 21 April 2023 doi:10.20944/preprints202304.0693.v1

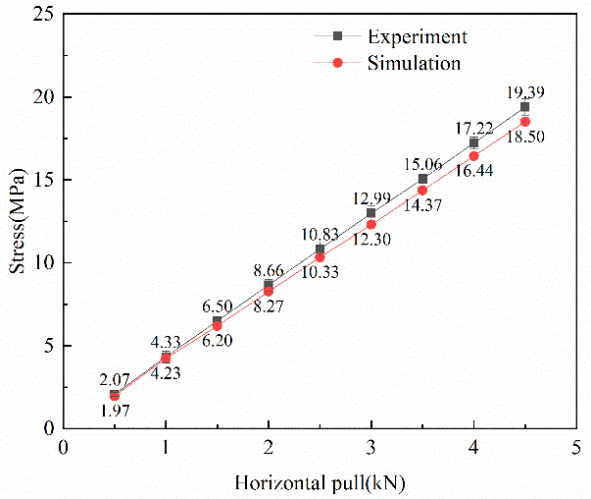


**Figure 9.** Stress comparisons in the bottom of the core rod with different horizontal tension.

*2.4. Experimental verification of vibration characteristics*

In this section, based on a single insulator and two series insulators, vibration characteristics tests are carried out to verify the simulation model further. As shown in Fig. 10, two identical composite post insulators are fixed on the vibrating table through steel plates. An acceleration measuring point is arranged on the vibrating table. Two acceleration measuring points are arranged on the top and bottom of 1 # and 2 # insulators, respectively. A strain flower is arranged at the bottom of the insulator, and a vertical strain gauge is arranged on the opposite side at the bottom of the mandrel. The specific measuring point arrangement is shown in Fig. 11. In the dynamic characteristics test of a single insulator, the white noise of 0.1g-0.4g amplitude in X and Y directions is input through the vibration test bench. The test conditions are shown in Table 5.

The dynamic characteristics test of 1 # and 2 # insulator vertical connection ( 2 # insulator above, 1 # insulator below ). The specific test conditions are shown in Table 6.

The modal analysis is carried out simultaneously based on the finite element model of the single insulator and the two insulators connected in the upper section. As shown in Table 7, the comparison results show that the simulation results of the first two frequencies of the insulator are consistent with the test results, and the deviation range is within 3 %. The insulator simulation model constructed in this paper agrees with the engineering practice.

**Table 5.** Dynamic Performance Test Condition of Insulators 1# and 2#

| Condition | Incoming wave | Amplitude | Frequency range Duration | Horizontal direction |
|---|---|---|---|---|
| 1-X\Y | white noise | 0.1g | 1-100Hz 180s | X\Y |
| 2-X\Y | | 0.2g | | |
| 3-X\Y | | 0.3g | | |
| 4-X\Y | | 0.4g | | |

Preprints (www.preprints.org) | NOT PEER-REVIEWED | Posted: 21 April 2023 doi:10.20944/preprints202304.0693.v1

**Figure 10.** Dynamic performance test.

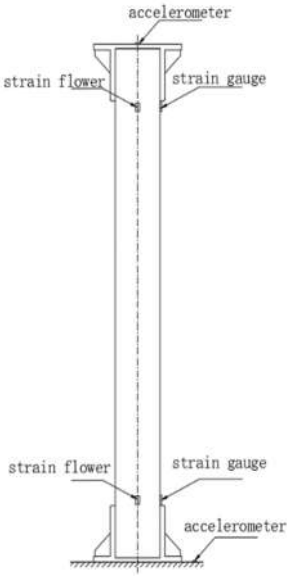


**Figure 11.** Schematic drawing of test point.

**Table 6.** Dynamic Performance Test Condition of Two Insulators in Series

| Condition | Incoming wave | Amplitude | Frequency range Duration | Horizontal direction |
|---|---|---|---|---|
| 5-X\Y\Z | white noise | 0.1g | 1-100Hz | X\Y\Z |
| 6-X\Y\Z | | 0.2g | 180s | |

Preprints (www.preprints.org) | NOT PEER-REVIEWED | Posted: 21 April 2023 doi:10.20944/preprints202304.0693.v1

**Table 7.** Comparison of simulation analysis and shaking table test in two types of insulators

| | | The first order natural frequency/Hz | 2nd order natural frequency/Hz |
|---|---|---|---|
| Single insulator | simulation | 12.50 | 87.90 |
| | experiment | 12.20 | / |
| | deviation /% | 2.50 | / |
| Two insulators in series | simulation | 3.26 | 19.69 |
| | experiment | 3.23 | 19.30 |
| | deviation /% | 1.0 | 2.0 |

## 2. Optimization Design of Flange Structure Parameters

Based on the above conclusions, the structural parameters of the flange are optimized. This section examines the static stimulation and modal analysis of a single insulator and two insulators in series, respectively. In the static simulation, the bottom of the flange is fixed, and a horizontal tension of 10 kN is applied along the top of the insulator to analyze the stress of the insulator under the horizontal tension.

According to the manufacturing process of the flange, the thickness of the flange is generally 10 mm~20 mm. Therefore, flange thickness increases from 10 mm to 20 mm with each gradient of 2.5 mm, and flange height increases from 165 mm to 205 mm with each gradient of 10 mm.

The natural frequency characteristics of the insulator under different flange heights and thicknesses are explored when the height of the insulator stiffener ( non-pressed area ) is constant. Fig. 12 and Fig. 13 show the simulation results of the first two natural frequencies of the insulator under different flange structure parameters.

It can be seen from the diagram that whether it is a single insulator or two insulators in series, the influence of flange height and thickness on the first two natural frequencies is not apparent when the height of the insulator stiffener ( non-pressed area ) is constant. The first two natural frequencies are positively correlated with horizontal stiffness. It can be seen that when the height of the insulator stiffener ( non-pressed area ) is constant, the change of flange height and thickness parameters has little effect on the horizontal stiffness of the insulator.

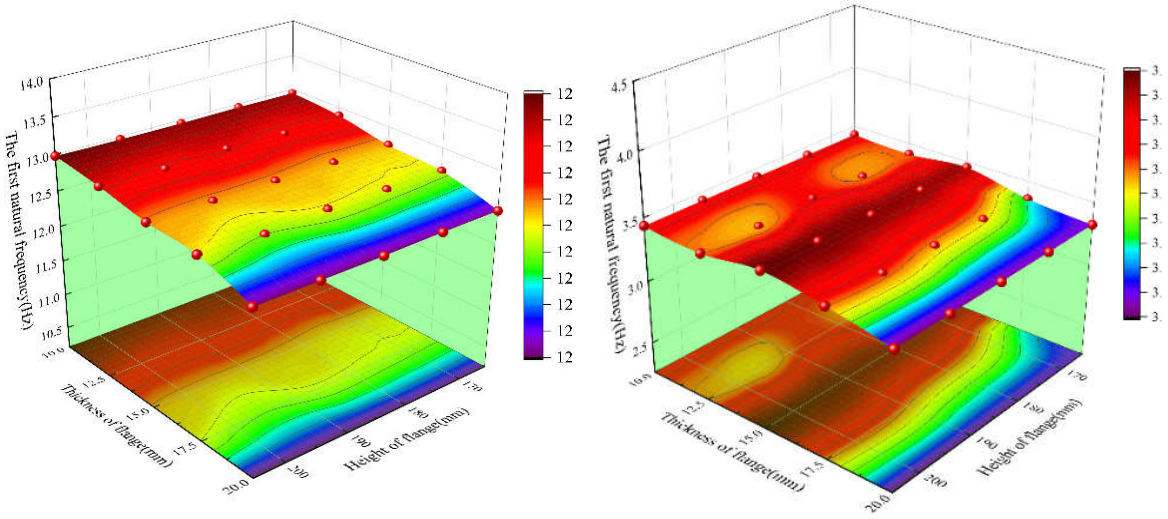


(a) (b)

**Figure 12.** The first order frequency (a) Single insulator (b) Two insulators in series.

Preprints (www.preprints.org) | NOT PEER-REVIEWED | Posted: 21 April 2023 doi:10.20944/preprints202304.0693.v1

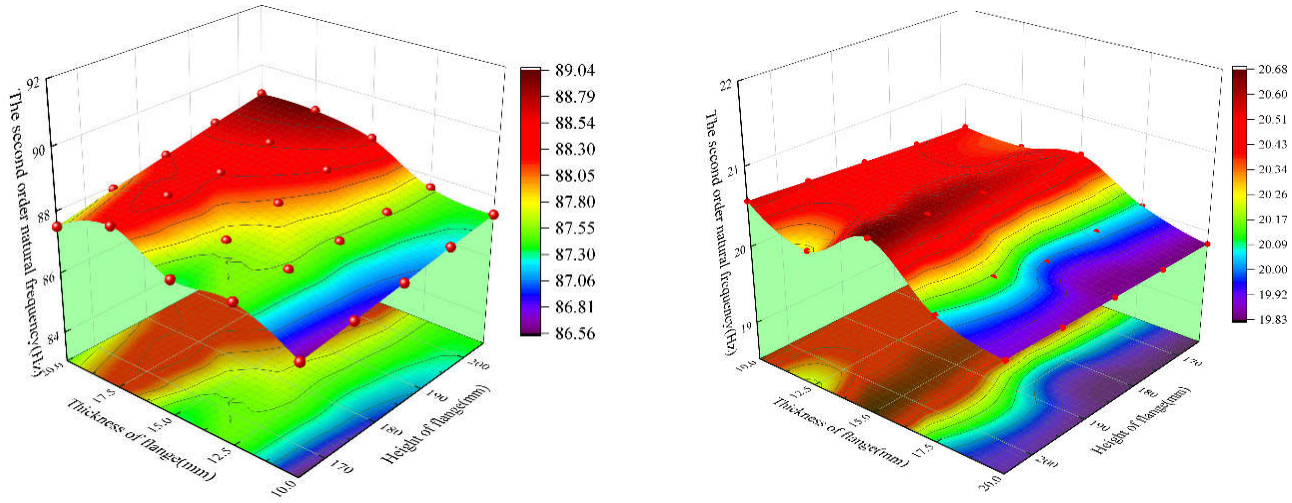


(a) (b)

**Figure 13.** The second order frequency (a) Single insulator (b) Two insulators in series.

Fig.14 (a) is the maximum horizontal displacement diagram of a single insulator, and Fig.14 (b) is the maximum stress diagram of a single insulator. The simulation results show that the maximum horizontal displacement of the insulator occurs at the top flange, and the maximum stress of the insulator occurs at the top of the flange stiffener, that is, the junction of the flange crimping area and the non-crimping area. The maximum horizontal displacement can reflect the horizontal stiffness of the insulator, and the maximum stress is the maximum value of the stress concentration area when the insulator is stressed. The smaller the maximum stress value, the higher the safety margin.

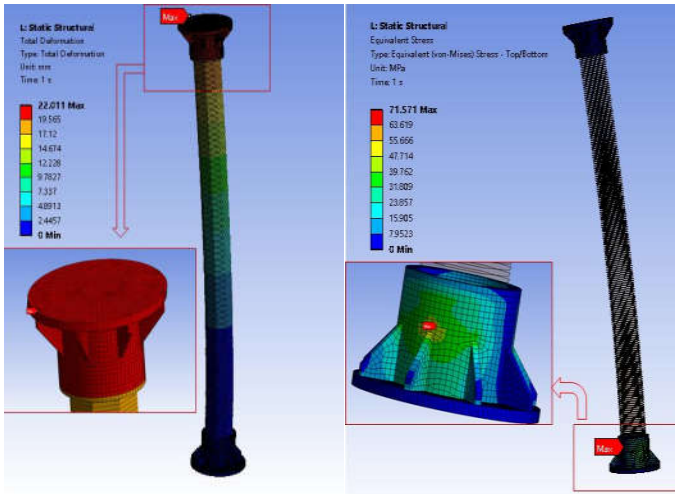


(a) (b)

**Figure 14.** (a) Max. horizontal displacement (b) Max. stress of the insulator.

Fig. 15 and Fig. 16 are the insulator's maximum horizontal displacement and maximum stress diagram, respectively. When the flange thickness is 10mm, in the case of a single insulator, as the flange height increases from 165 mm to 205 mm, the maximum horizontal displacement of the insulator decreases from 23.6 mm to 23 mm, with a decrease of 2.5 %. In the case of two insulator strings, the downward trend is the same, from the maximum horizontal displacement of 195 mm to 190.4 mm, a decrease of 2.4 %. It can be seen that when the flange thickness of the two insulators is constant and the height of the insulator stiffener ( non-pressing area ) is constant, the maximum horizontal displacement decreases by less than 3 % with the increase of flange height.

Preprints (www.preprints.org) | NOT PEER-REVIEWED | Posted: 21 April 2023 doi:10.20944/preprints202304.0693.v1

In the case of a single insulator, when the height of the flange is fixed at 205 mm, as the flange thickness increases from 10 mm to 20 mm, the maximum horizontal displacement of the insulator decreases from 23 mm to 21.8 mm, with a decrease of 5.2 %. In the case of two insulator strings, the maximum horizontal displacement decreased from 190.4 mm to 183.35 mm, a decrease of 3.7 %. It can be seen that when the flange height of the two insulators is constant, the maximum horizontal displacement decreases slightly with the increase of flange thickness, and the decrease is about 5 %. Based on the above analysis, it can be seen that the change in flange height and thickness parameters has little effect on the change of horizontal stiffness, which is consistent with the above natural frequency conclusion..

Combined with the maximum stress diagram analysis of the two insulators, when the flange thickness is constant, the maximum stress value is unchanged when the height of the flange crimping zone changes. That is, the height of the flange crimping zone does not affect the bending resistance of the insulator. When the flange height is 205 mm, in the case of a single insulator, the flange thickness increases from 10 mm to 20 mm, and the maximum stress value decreases from 158.7 MPa to 72.3 MPa, with a decrease of 54.4 %. In the case of two insulator strings, the maximum stress value decreased from 322 MPa to 146.6 MPa, a decrease of 54.4 %. It can be seen that within the specified range of the crimping process, the thicker the flange, the smaller the maximum bending stress. Its bending strength is more significant, and the safety margin is more incredible.

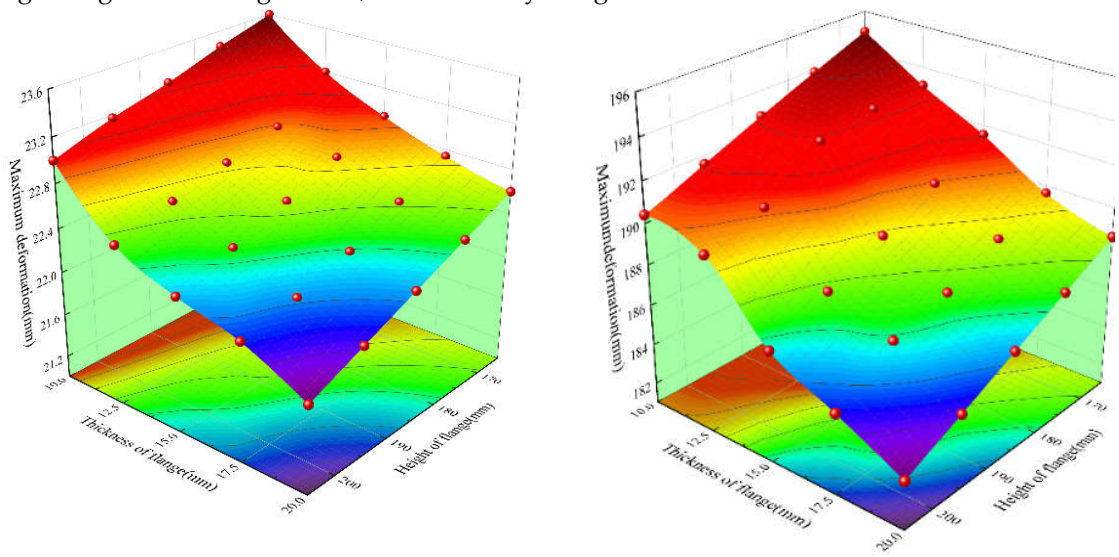


(a) (b)

**Figure 15.** Max. horizontal displacement of the insulator (a) Single insulator (b) Two insulators in series.

Preprints (www.preprints.org) | NOT PEER-REVIEWED | Posted: 21 April 2023 doi:10.20944/preprints202304.0693.v1

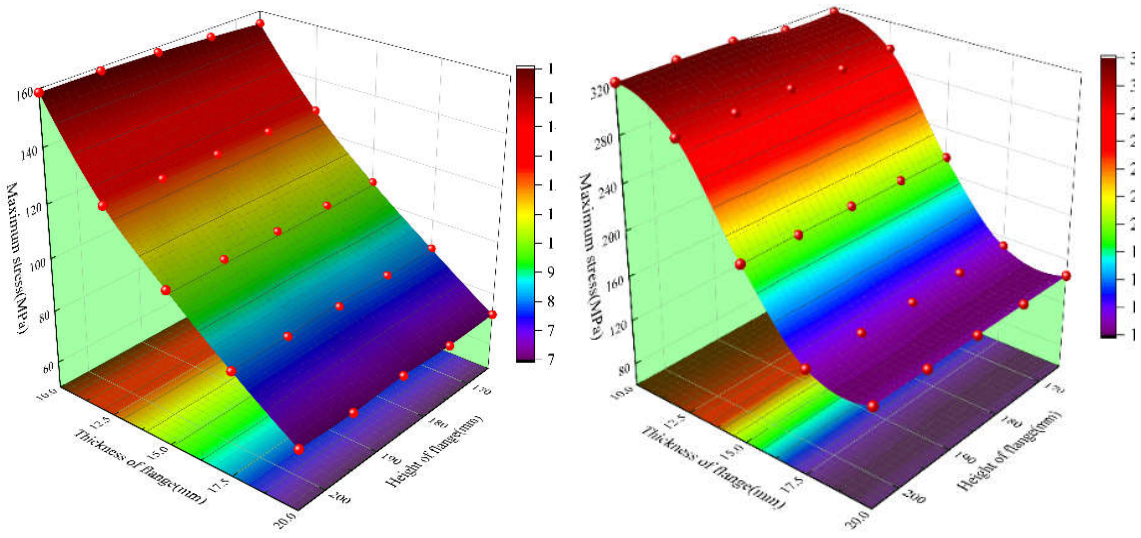


(a) (b)

**Figure 16.** Max. stress of the insulator (a) Single insulator (b) Two insulators in series.

## 3. Conclusion

This paper studies the crimped composite post-insulator widely used in flexible DC converter valves. The MPC local constraint method is used to simulate the crimping process of the insulator mandrel and flange, and the simulation model of the new crimped insulator is constructed. The material mechanics equivalent calculation, shaking table dynamic characteristic test, and static tensile test of the composite post insulator is carried out, and the rationality of the model is demonstrated. Based on the above model, the structural parameters of the flange are optimized, and the influence of flange height and thickness on the mechanical properties of the insulator is explored. The main conclusions are as follows :

- The MPC local constraint modeling method of ANSYS software is used to simulate the flange crimping process of composite post insulator. The difference between the simulation and test results is less than 5 %. The simulation analysis method can be applied to the finite element simplified modeling of the post-insulator in the flexible DC converter valve.
- When the height of the insulator stiffener ( non-pressing area ) is constant, the influence of flange height and flange thickness on the horizontal stiffness of the insulator can be ignored. When the flange height and thickness change, the natural frequency of the insulator does not change significantly. In static analysis, the change of flange height and thickness has little effect on the maximum offset of the insulator, and the deviation range is within 5 %.
- When the height of the insulator stiffener ( non-pressing area ) is constant, the change in flange thickness significantly affects the insulator's bending performance. The thicker the crimped composite post-insulator flange is, the smaller the maximum bending stress, and the maximum decrease is 54.4 %. That is, the increase in flange thickness can significantly increase the bending resistance of the insulator.
- In the production of the crimping insulator, the height of the flange is reduced as much as possible under the condition of process permission. The increase in flange height not only increases the cost but also reduces the dry arc distance of the insulator. More importantly, the influence of the flange height on the bending strength of the insulator can be ignored.

**Author Contributions:** Conceptualization, J.X.; methodology, J.X.; software, Y.Z.; validation, J.X., Y.Z. and Y.X.; formal analysis, Y.J.; investigation, Y.J.; resources, Y.J.; data curation, J.X.; writing—original draft preparation, J.X.; writing—review and editing, Y.Z., L.Z.; visualization, Y.Z.; supervision, Y.X.; project administration, J.X.; funding acquisition, J.X. All authors have read and agreed to the published version of the manuscript.

**Funding:** This research was funded by the National Key R&D Program of China 2021YFB2400603.

**Data Availability Statement:** The data presented in this study are available on request from the corresponding author.

**Conflicts of Interest:** The authors declare no conflict of interest.

## References


1. Ang, A. H.-S., J. A. Pires, and R. Villaverde. "A Model for the Seismic Reliability Assessment of Electric Power Transmission Systems." *Reliability Engineering \& System Safety* 51, no. 1 (1996): 7-22.
2. Arrillaga, Jos, Neville R. Watson, and Y. H. Liu. *Flexible Power Transmission: The Hvdc Options*: John Wiley \& Sons, 2007.
3. Park, R., I. J. Billings, G. C. Clifton, J. Cousins, A. Filiatrault, D. N. Jennings, L. C. P. Jones, N. D. Perrin, S. L. Rooney, and J. Sinclair. "The Hyogo-Ken Nanbu Earthquake (the Great Hanshin Earthquake) of 17 January 1995: Report of the Nznsee Reconnaissance Team." *Bulletin of the New Zealand Society for Earthquake Engineering* 28, no. 1 (1995): 1-98.
4. Sokolov, Vladimir, and Friedemann Wenzel. "On the Modeling of Ground-Motion Field for Assessment of Multiple-Location Hazard, Damage, and Loss: Example of Estimation of Electric Network Performance During Scenario Earthquake." *Natural hazards* 74, no. 3 (2014): 1555-75.
5. Christensen, Richard M. *Mechanics of Composite Materials*: Courier Corporation, 2012.
6. Epackachi, S., K. M. Dolatshahi, N. D. Oliveto, and A. M. Reinhorn. "Mechanical Behavior of Electrical Hollow Composite Post Insulators: Experimental and Analytical Study." *Engineering structures*, no. 93-Jun.15 (2015).
7. Xidong, Liang, Wang Shaowu, Fan Ju, and Guan Zhicheng. "Development of Composite Insulators in China." *IEEE Transactions on Dielectrics and Electrical Insulation* 6, no. 5 (1999): 586-94.
8. Huang, Haimeng, Yunqiang Xu, Huan Li, Zimin Zhang, Yuke Li, Haoyue Zhang, Junji Cheng, Bo Yi, Zhiming Wang, and Guoyi Zhang. "Optimization and Comparison of Specific on-Resistance for Superjunction Mosfets Considering Three-Dimensional and Insulator-Pillar Concepts." *IEEE Transactions on Electron Devices* 69, no. 3 (2022): 1162-68.
9. Mohammadi, R. Karami, V. Akrami, and F. Nikfar. "Dynamic Properties of Substation Support Structures." *Journal of Constructional Steel Research* 78 (2012): 173-82.
10. Moustafa, Mohamed A., and Khalid M. Mosalam. "Structural Performance of Porcelain and Polymer Post Insulators in High Voltage Electrical Switches." *Journal of Performance of Constructed Facilities* 30, no. 5 (2016): 04016002.
11. Wen, Bo, and Di Tao Niu. "Seismic Response Analysis of Substation Involving Interaction of Main Structure-Electrical Equipments." Paper presented at the Advanced Materials Research 2011.
12. Rowland, S. M., J. Robertson, Y. Xiong, and R. J. Day. "Electrical and Material Characterization of Field-Aged 400 Kv Silicone Rubber Composite Insulators." *IEEE Transactions on Dielectrics and Electrical Insulation* 17, no. 2 (2010): 375-83.
13. Tedesco, Joseph, William G. McDougal, and C. Allen Ross. *Structural Dynamics*: Pearson Education London, UK, 2000.
14. Cimellaro, G. P., A. M. Reinhorn, and A. Schiff. "Evaluation of Hollow Core Composite Insulators." In *Tclee 2009: Lifeline Earthquake Engineering in a Multihazard Environment*, 1-12, 2009.
15. Cimellaro, G. P., H. Roh, M. Fahad, A. M. Reinhorn, and A. Schiff. "Modeling Combined Friction-Viscous Damping in Response of Hollow Core Composite Insulators." In *Structures Congress 2010*, 2736-47, 2010.

16. Hong, Rao, Luo Bing, Xiaolin Li, Cai Zongyuan, and Licheng Li. "Development of ± 800kv Uhvdc Transmission Technology in China." Paper presented at the 2008 International Conference on High Voltage Engineering and Application 2008.
17. Liang, Xidong, Weining Bao, and Yanfeng Gao. "Decay-Like Fracture Mechanism of Silicone Rubber Composite Insulator." *IEEE Transactions on Dielectrics and Electrical Insulation* 25, no. 1 (2018): 110-19.
18. Faliang, H. E. "Development of Crimped Composite Post Insulator with Large Diameter Core Rod [J]." *Insulators and Surge Arresters* 2 (2020): 222-28.
19. Safonov, Alexander, Mikhail Gusev, Anton Saratov, Alexander Konstantinov, Ivan Sergeichev, Stepan Konev, Sergey Gusev, and Iskander Akhatov. "Modeling of Cracking During Pultrusion of Large-Size Profiles." *Composite Structures* 235 (2020): 111801.
20. Volk, Maximilian, Joanna Wong, Shelly Arreguin, and Paolo Ermanni. "Pultrusion of Large Thermoplastic Composite Profiles up to 40 Mm from Glass-Fibre/Pet Commingled Yarns." *Composites Part B: Engineering* 227 (2021): 109339.
21. Zhang, Jie, Li Jiang, Zhengyi Huang, Xuesong Xu, Peng Wu, and Hong Lei. "Seismic Analysis under Sl-1 of New Structure Support Frame for Iter Pf Converter System." *IEEE Transactions on Plasma Science* 50, no. 11 (2022): 4355-60.
22. Shiling, Zhang. "Research on Operation Characteristics of Uhv Converter Valve Hall Based on Intelligent Image Processing and 3d Modeling Technology." Paper presented at the Journal of Physics: Conference Series 2021.
23. Yang, Zhenyu, Qiang Xie, Yong Zhou, and Khalid M Mosalam. "Seismic Performance and Restraint System of Suspended 800 Kv Thyristor Valve." *Engineering structures* 169 (2018): 179-87.
24. Hasegawa, T, K Yamaji, H Irokawa, H Shirahama, C Tanaka, and K Akabane. "Development of a Thyristor Valve for Next Generation 500 Kv Hvdc Transmission Systems." *IEEE transactions on power delivery* 11, no. 4 (1996): 1783-88.
25. Liang, Huangbin, and Qiang Xie. "System Vulnerability Analysis Simulation Model for Substation Subjected to Earthquakes." *IEEE transactions on power delivery* 37, no. 4 (2021): 2684-92.
26. He, Chang, Lizhong Jiang, and Liqiang Jiang. "Seismic Failure Risk Assessment of Post Electrical Equipment on Supporting Structures." *IEEE transactions on power delivery* (2023).